9-16-2018

Localization Effects on the Dissipation of Gravity Wave Packets in the Upper Mesophere and Lower Thermosphere

C. J. Heale
Embry-Riddle Aeronautical University, HEALEC@erau.edu

R. L. Walterscheid
The Aerospace Corporation

J. B. Snively
Embry-Riddle Aeronautical University, snivelyj@erau.edu

Journal of Geophysical Research: Atmospheres

RESEARCH ARTICLE
10.1029/2017JD027617

Localization Effects on the Dissipation of Gravity Wave Packets in the Upper Mesosphere and Lower Thermosphere

C. J. Heale[1], R. L. Walterscheid[2], and J. B. Snively[1]

[1]Center for Space and Atmospheric Research, Department of Physical Sciences, Embry-Riddle Aeronautical University, Daytona Beach, FL, USA, [2]Space Science Applications Laboratory, The Aerospace Corporation, El Segundo, CA, USA

Key Points:
- Gravity wave packets are strongly attenuated by dispersion before they reach the dissipative thermosphere
- The central λ_z of a packet with broad spectra tends to evolve toward smaller values in time
- Wave packets generated in dissipative regions, with wavelengths smaller than the scale height, can evolve to longer vertical wavelengths

Supporting Information:
- Supporting Information S1
- Supporting Information S2

Correspondence to:
C. J. Heale,
healec@erau.edu

Citation:
Heale, C. J., Walterscheid, R. L., & Snively, J. B. (2018). Localization effects on the dissipation of gravity wave packets in the upper mesosphere and lower thermosphere. *Journal of Geophysical Research: Atmospheres*, *123*, 8915–8935. https://doi.org/10.1029/2017JD027617

Received 23 AUG 2017
Accepted 5 JUL 2018
Accepted article online 3 AUG 2018
Published online 2 SEP 2018

Abstract Gravity waves not subject to breaking or filtering will dissipate due to viscosity and thermal conduction in the thermosphere. However, the evolutions of wave packets, and the altitudes they reach, are highly dependent upon the spectral content. In this paper, a 2-D numerical model is used to investigate the effect of spatial localization (and thus spectral content) of a wave packet on its dissipation, dispersion, and spectral evolution. It is found that most wave packets launched below the thermosphere evolve to smaller central vertical wavelengths as the faster, longer vertical wavelength components reach the dissipative thermosphere and are removed first, leaving the shorter, slower components to become dominant at later times. This effect is greater for more spatially localized packets (spectrally broadband) as rapid dispersion leads to the rapid spreading of the wave over large altitude regions that could be interpreted as different waves (i.e., from different sources) by instruments observing different altitudes. Dispersion can also be accelerated by the refractive effects of the thermospheric temperature gradient. Initially, Gaussian broadband packets can evolve into asymmetric distributions which are not well described by standard assumptions (e.g., Gaussian packets), requiring instead numerical simulation to properly describe them. In the case that the vertical scale is smaller than the scale height, and dissipation acts immediately on the packet (i.e., it is generated in situ in the dissipative thermosphere), then the scale-dependent nature of dissipation removes the shorter wavelengths components first, leading to the spectrum evolving toward larger vertical wavelengths.

1. Introduction

Internal gravity waves provide an important mechanism for transporting energy and momentum from lower atmospheric sources to the middle and upper atmosphere (e.g., Fritts & Alexander, 2003; Hocke & Tsuda, 2001; Hung & Kuo, 1978; Lindzen, 1981; Vincent & Reid, 1983; Yiğit & Medvedev, 2015). The energy and momentum is deposited into the mean state primarily via dissipation, critical level filtering, transience, and wave breakdown. The deposition of momentum, sensible heat, and energy can accelerate/decelerate the mean flow and heat/cool the atmosphere (Fritts & Alexander, 2003; Holton, 1982, 1983; Lindzen, 1981; Pitteway & Hines, 1963; Walterscheid, 1981; Yiğit et al., 2008, 2009; Vadas & Liu, 2009, 2013). This leads to important consequences for the atmospheric circulation, such as the quasi-biennial oscillation and the cold summer mesopause (Alexander & Rosenlof, 1996; Baldwin et al., 2001; Fritts & Alexander, 2003; Garcia & Solomon, 1985; Holton & Alexander, 2000). The deposition of momentum can also generate secondary waves, which continue to propagate to higher altitudes, via two main mechanisms. Secondary waves can arise as a linear response to the body forcing of a dissipating primary wave and tend to have scales larger than the primary wave (e.g., Vadas et al., 2003; Vadas & Fritts, 2002, 2006; Vadas et al., 2014). Secondary waves can also be generated nonlinearly through breaking as wave energy cascades to smaller scales (e.g., Bossert et al., 2017; Fritts & Lund, 2011; Heale et al., 2017; Snively & Pasko, 2008; Vincent et al., 2013).

A question of fundamental importance is the altitude to which waves originating in the lower atmosphere and reaching the thermosphere may propagate before they dissipate by viscous dissipation higher in the thermosphere. For waves that do not break down or encounter critical levels, the primary mechanisms by which wave packets attenuate is through wave packet dispersion and scale-dependent dissipation (viscous dissipation) Viscous dissipation is a function of the phase speed and vertical wavelength of the wave, with larger values of both being able to propagate higher (e.g., Pitteway & Hines, 1963; Vadas & Fritts, 2005; Vadas, 2007). For linear, steady state waves, only scale-dependent dissipation contributes to the diminishment of

wave amplitude; however, gravity waves are never fully monochromatic and can be generated as packets with varying spectral content. More impulsive sources generate broader spectra of waves. For dispersive waves, the broader the spectrum (the broader the range of phase speeds) the more dispersive the packet is (Jackson, 1975; Lighthill, 1965; Walterscheid, 2013).

Previous studies have considered the dissipation of waves using theoretical, numerical, and ray tracing approaches (Heale et al., 2014; Hickey et al., 1998; Liu et al., 2013; Vadas, 2007; Vadas & Fritts, 2005; Vadas & Liu, 2009, 2013; Vadas & Nicolls, 2012; Vadas et al., 2015; Walterscheid, 2013; Waterscheid & Hickey, 2011; Zhang & Yi, 2002) and have highlighted that the bandwidth of the packet has very important consequences for wave attenuation and the spectral evolution. In the steady state (monochromatic) limit, dissipation leads to increasing wavelength with altitude (Heale et al., 2014; Hickey et al., 1998) since viscosity acts to preferentially remove smaller scales at any given altitude. Therefore, the vertical wavelength gets progressively longer as altitude increases. It is noted that the measured values of gravity wave vertical wavelengths increase exponentially in altitude (Djuth et al., 2004; Heale et al., 2014; Oliver et al., 1997; Vadas, 2007), in general, for waves in the thermosphere. However, the steady state limit, by its nature, omits the time-dependent effects of dispersion.

For transient wave packets, wave dispersion can lead directly to diminished wave packet amplitudes, by spreading the wave energy over an increasingly larger volume. This goes as $\sim t^{n/2}$ where n is the number of dimensions over which the packet has a finite bandwidth (Lighthill, 1965). In addition, dispersion can also lead to the faster, longer vertical wavelength components of a packet reaching the thermosphere first and dissipating first, leaving the slower, shorter vertical wavelength components to become dominant at later times. This effect causes the shift in the dominant vertical wavelength to smaller values in time and slows the upward progress of the packet (Heale et al., 2014; Vadas et al., 2015). Alternatively, wave packets that remain coherent can attenuate by scale-dependent dissipation before they disperse and are thus subject to selective removal of the short-scale waves making up the wave packet. This process shifts the central wave number to smaller wave numbers (longer wavelengths) and accelerates the upward propagation of the packet (Walterscheid, 2013). However, the limit at which each of these spectral evolutions occur is currently not well understood.

Clearly then, the dissipation of a wave and its spectral evolution are heavily influenced by the bandwidth (the localization or impulsiveness) of the wave packet and the environment in which a wave is launched. For most gravity wave drag parameterizations that include thermospheric dissipation, the steady state limit is assumed and dispersive effects are omitted. Ray trace theory relies on the concept of group velocity to define a wave's trajectory and does not include dispersive effects on amplitude explicitly unless a number of rays with different initial parameters are used to describe a packet (e.g., Vadas & Liu, 2009, 2013; Vadas et al., 2015). Unless a set of rays is initialized to reproduce the spectral nature of a wave packet, including especially its bandwidth, ray tracing is subject to assumptions of weak dispersion and governed by Wentzel-Kramers-Brillouin (WKB) theory (i.e., that the viscosity and diffusivity are locally constant and that the vertical scale is small when compared to the scale of temperature and wind variations in the atmosphere), which may not hold well for waves that reach the thermosphere from the lower atmosphere.

In this paper, we extend the work of Heale et al. (2014) to examine the effects of bandwidth and launch altitude on the combined effects of dispersion and dissipation, and extend the work of Walterscheid (2013) using a more realistic model of wave propagation. In addition, we examine the relative effects of dispersion and dissipation in diminishing wave amplitude. The 2-D fully compressible numerical model of Snively and Pasko (2008) is used to investigate the dispersion and dissipation of gravity wave packets of different spatial localizations (bandwidth), and to determine in which limits the central wavelength of the packet is shifted to larger or smaller values. We present simulations based upon the wave parameters of Walterscheid (2013) and vary the spatial localization, launch altitude, and central vertical wavelength in order to investigate the relative effects of dispersion and dissipation and their relative importance in wave packets of differing spectral bandwidth. We also examine the effects of realistic thermal structure.

The paper is laid out as follows: Section 2 described the numerical model used and the case studies that are simulated, section 3 describes the state of the initial ambient atmosphere, section 4 presents and discusses the results from the case studies, and finally, section 5 presents the summary and conclusions.

Table 1
Table Showing the Initial Parameters Used for Each of the Cases Studied

Case	λ_x (km)	λ_z (km)	Packet FWHM (vertical wavelengths)	z_0 (km)
1	40	10	1	40
2	40	10	3	40
3	40	10	1	80
4	40	10	3	80
5	40	5	1	80
6	40	5	3	80
7	40	5	1	120
8	40	5	3	120
9	40	10	1	120
10	40	10	3	120
11	40	5	1	40
12	40	5	3	40
13	40	10	1	40
14	40	10	3	40

Note. Cases 1 – 10 propagate through an isothermal atmosphere, while cases 11 – 14 propagate through an atmosphere with a realistic thermosphere. FWHM = full width at half maximum.

2. Numerical Model and Case Studies

The simulations and cases studies in this paper are performed using the 2-D nonlinear, compressible model first described in Snively and Pasko (2008). This model uses a finite volume approach (LeVeque, 2002) to solve the Euler equations with the inclusion of gravity using the *f* wave method of Bale et al. (2002). The dissipative terms are solved using a time-split approach where the velocity and temperature are passed to a separate explicit solver after the main system of hyperbolic terms have been solved at each time step. An adaptive time step is used to ensure stability for both methods. A full description of the model used can be found in Snively and Pasko (2008) and Heale et al. (2014).

Wave packets are initialized by the following horizontal velocity perturbation:

$$u'(x,z,0) = A \cdot \exp\left(-\frac{(z-z_0)^2}{2\sigma_z^2} + \frac{(z-z_0)}{2H}\right) \cdot \exp(i(kx - m(z-z_0))), \quad (1)$$

where A is the amplitude (m/s), z_0 is the launch altitude, σ_z is the Gaussian width in altitude, H is the scale height, k is the horizontal wave number, and m is the vertical wave number. The other primitive variables are then specified using the gravity wave polarization relations (Fritts & Alexander, 2003). For waves that are initialized in the highly viscous region ($z = 120$ km), a complex frequency is defined by $\omega^* = \omega + i\alpha$, where $\alpha = (k^2 + m^2 - 1/4H^2)\nu$ and ν is the kinematic viscosity or molecular diffusivity, considered equal (i.e., the Prandtl number = 1; Vadas & Fritts, 2005). Under WKB assumptions, the kinematic viscosity is considered to be locally constant when deriving this result. With ω replaced by ω^*, the anelastic dispersion relation is solved for ω.

Each of the run parameters are presented in Table 1 The horizontal wavelength is 40 km for each case and σ_x is effectively infinite. The vertical wavelength is either 5 km (less than the scale height), or 10 km (approximately equal to the scale height) to assess how the WKB assumption, that the vertical scale is smaller than the scale height, affects the dispersion and dissipation. The spectral bandwidth is controlled by varying the initial localization of the packet. Wave packets are chosen such that the initial full width at half maximum (FWHM) encompasses either one (spatially narrow, spectrally broadband) or three (spatially broad, spectrally narrowband) vertical wavelengths (where FWHM $\sim 2.35\sigma_z$), this allows for an assessment of how the dispersion (which will be much greater for the spatially narrow, spectrally broadband cases) affects the evolution of the wave packet. The launch altitude (z_0) is changed in order to control the amount that the wave packet can disperse before it reaches the dissipative region of the thermosphere. In each case, the amplitude A is set to 1×10^{-3} m/s to maintain linearity.

3. Background Atmosphere

3.1. Isothermal Cases

The majority of the case studies shown here use an isothermal atmosphere for simplicity and using parameter values to compare with the results of Walterscheid (2013). The temperature is constant with a value of $T = 403$ K, leading to a density scale height $H = RT/g = 11.7$ km. The density profile is given by

$$\rho(z) = \rho_0 \exp(-z/H) \tag{2}$$

while the pressure is related to the density and temperature via the ideal gas law $p(z) = \rho(z)RT$, where $\rho_0 = 1.2$ kg/m^3, and $R = 287$ J/kg/K. The molecular kinematic viscosity profile is given by

$$\kappa(z) = \kappa_0 \frac{\rho(z)}{\rho_0)} \tag{3}$$

where $\kappa_0 = 3.79$e-2 m^2/s and is chosen such that $\kappa = 1{,}000$ m^2/s at $z = 120$ km, which is consistent with the $z = 120$ km viscosity in Walterscheid (2013) and Waterscheid and Hickey (2011). The Prandtl number is set to 1, such that the thermal conductivity is equal to the molecular viscosity.

The domain size is equal to the horizontal wavelength of the wave being simulated (40 km) in the x direction and has periodic boundary conditions, effectively making the wave monochromatic in k space. The vertical domain ranges from the ground to 170 km altitude with an open top boundary and a closed (reflecting) bottom boundary. The resolution in the horizontal direction is always 40 points per wavelength, and is 125 m in the vertical direction.

3.2. Realistic Thermosphere

In the final four cases, the temperature structure of the atmosphere is specified such that it is isothermal ($T = 240$ K) below 100-km altitude but features a realistic transition to $T = 1{,}000$ K in the thermosphere (e.g., Vadas & Fritts, 2006). The temperature is specified by

$$T(z) = T_{\max} + (T_0 - T_{\max}) \cdot \left[0.5 \cdot \left(1 - \tanh\left(\frac{z - z_\Delta}{\Delta}\right)\right)\right]^\beta \tag{4}$$

where $T_{\max} = 1000$ K, $T_0 = 240$ K, $z_\Delta = 116$ km, $\Delta = 17$ km, and $\beta = 0.19$. The density is given by the same equation as (2) but calculated with the vertical integral of z/H. The profiles for the realistic thermosphere cases are shown in Figure 1.

The only difference between the isothermal and realistic thermosphere simulation domains is that the vertical extent ranges from ground to 250 km in the realistic thermosphere simulations.

4. Results

The results for each case are presented in terms of a few metrics: (1) The time evolution of the wave packet is presented into terms of the density-weighted horizontal velocity ($u(z)'(\rho(z)/\rho(z_0))^{1/2}$) and are normalized to the initial maximum value. A vertical slice is taken at the mid x point of each domain at each time and placed sequentially to form the time series evolution. (2) The altitude and amplitude of maximum energy density is plotted at each time to follow the *center* of the wave packet and assess the decay in wave amplitude. For each case, an inviscid version of the simulation is also run and the amplitude of the maximum energy density is plotted. Therefore, the effects of dispersion and dissipation on the energy density can be separated. The energy density is given by (Walterscheid, 2013)

$$E = \frac{1}{2}\rho\left[\overline{\mathbf{u}'^2} + \frac{g^2}{N^2}\overline{\left(\frac{\theta'}{\overline{\theta}}\right)^2}\right] \tag{5}$$

where g is the acceleration due to gravity and θ is potential temperature, N is the buoyancy frequency and overbars denote horizontal averages. (3) Vertical wavelength spectra are measured along the energy density path as a function of time using a Morlet wavelet analysis (Torrence & Compo, 1998) to assess the evolution of the dominant wavelength. This is done by plotting the entire vertical wavelength power spectrum at the altitude of the maximum energy density at each time step. We compared results using this method with a Fourier transform (not shown) to ensure that wavelet localization does not bias the scales measured and found no significant difference. The Wavelet analysis has the advantage that the specific altitude of interest can be identified for each time step. The predicted inviscid vertical wavelength along the path of maximum

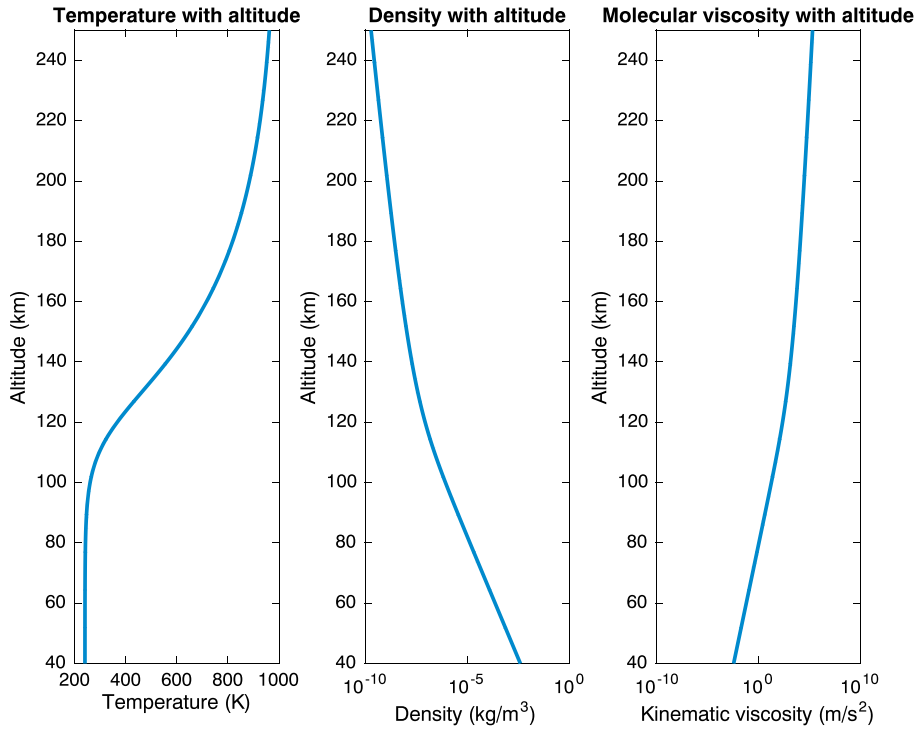

Figure 1. The ambient atmosphere profiles for (left) temperature, (middle) density, and (right) molecular viscosity for the realistic thermosphere simulations.

energy density is also overlaid on the vertical wavelength spectra plots measured from the simulation for cases 11–14. The predicted vertical wavelength is calculated by using the anelastic dispersion relation:

$$m^2 = \frac{k^2 N^2}{\omega^2} - k^2 - \frac{1}{4H^2} \tag{6}$$

where k is the horizontal wave number and the wave frequency ω is the (fixed) central wave packet frequency.

4.1. Cases 1–4

In Cases 1–4, we compare the propagation of a 40-km λ_x, 10-km λ_z wave packet that are launched from z = 40- and 80-km altitude, with one and three vertical wavelengths encompassed in the packet FWHMs, respectively. The former case is broadband and the latter is narrowband. Dispersion will be significantly more dramatic for more broadband packets; the initial Fourier spectral content is shown in Figure 2.

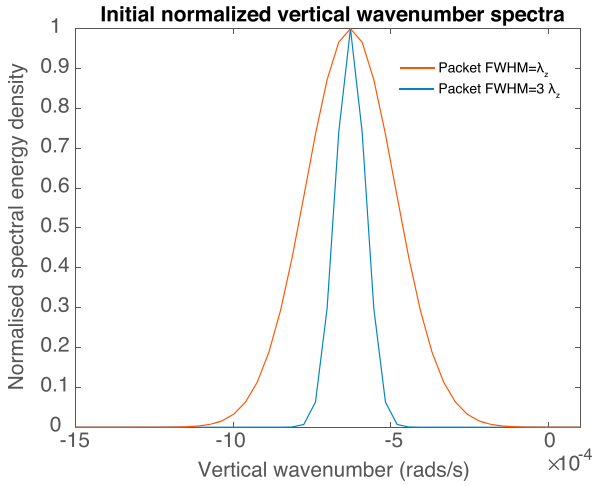

Figure 2. A comparison of the initial vertical wave number spectra (rads/m) for u' from packets that encompass one or three vertical wavelengths for wave parameters λ_x = 40 km, and λ_z = 10 km. The wave packet that includes one cycle is far broader than the one including three cycles. FWHM = full width at half maximum.

Figure 3 shows simulation results for Cases 1–4 showing (a) the scaled, normalized horizontal velocity over altitude as a function of time, with inviscid group velocity (i.e., using the initial, central m, and ω that remain constant in time) and maximum energy density paths overlaid, (b) the normalized vertical wavelength spectrum along the energy density path, and (c) the value of the maximum energy density with time. The inviscid group velocity is given by the following equation:

$$C_g = \frac{-m\omega}{k^2 + m^2 + 1/4H^2} \tag{7}$$

We begin our discussion with Case 1, where the launch altitude is 40 km and the initial packet width is 10 km. Case 1 (top left), panel (a) in Figure 3 shows that the spatially localized packet disperses rapidly in time and spans an altitude range of ~100 km after just 75 min. Beyond this time, dissipation starts to significantly reshape the packet as the leading edge (comprising high-frequency, long vertical wavelength components) is removed from the spectrum and the altitude span of the packet begins

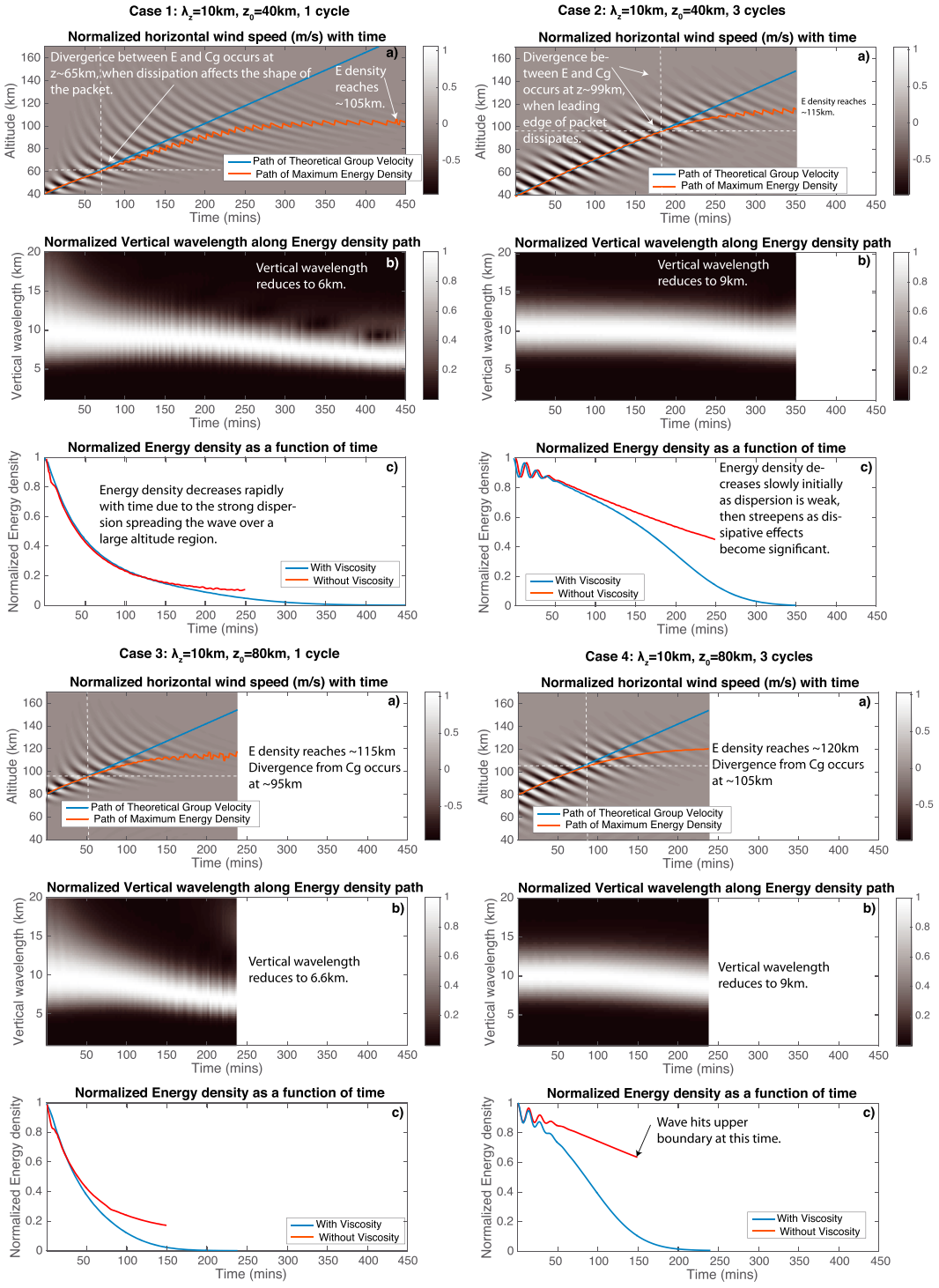

Figure 3. Simulation results for Cases 1–4 showing (a) the scaled, normalized horizontal velocity in Keogram form as a function of time, with inviscid group velocity and maximum energy density paths overlaid, (b) the normalized vertical wavelength spectrum, and (c) the value of the maximum energy density with time for viscous and inviscid version of the simulation.

to shrink. At this point, the group velocity and energy density paths begin to diverge as viscosity dissipates the leading edge of the packet and the vertical flow of energy ceases beyond ~300 min. It is key to note that the energy density path diverges from the group velocity path (the path the energy center would take in a nonviscous atmosphere) before either of them reach the viscous thermosphere (~100-km altitude). Therefore, the centrum of the packet can be significantly influenced by dissipation of the leading edge. If the wave packet in this case were represented by a single ray using ray trace theory, its path would not veer from the inviscid group velocity path until it reached the viscous thermosphere and would not well represent the energy density path shown in Figure 3, Case 1, panel (a). In fact, the packet becomes so dispersed that it would be impossible to describe using a single ray. Gravity wave drag parameterizations have similar difficulty representing spectrally broad packets. Most schemes that include thermospheric dissipation assume steady state conditions and instant propagation and as a result, the dispersion and time-dependent dissipation of the packet (and resulting time-dependent forcing of the thermosphere) would not be captured.

The vertical wavelength spectrum, shown in Figure 3, Case 1, panel (b), shows a shift in the dominant vertical wavelength from longer to shorter values as time progresses. This shift to smaller vertical wavelength occurs via the mechanism described in Heale et al. (2014) and results from strong dispersion. The fast, long vertical wavelength components reach the thermosphere first and are dissipated first, while the slower, shorter vertical wavelength components lag behind and dissipate at later times, hence the shift in dominant vertical wavelength from large to small values (this process is shown in more detail in Figure 6). When considering viscosity as a diffusion equation, the rate of amplitude decay is given by $\sim \nu m^2$. Therefore, packet components with shorter vertical wavelengths decay more rapidly than larger vertical wavelengths at the same altitude. This assumption, as made in Walterscheid (2013), requires that a packet remains coherent, the spectral components are dissipating at the same time, and the viscosity does not vary much over the packet span. These assumptions do not hold for spectrally broad cases. Strong dispersion leads to separation of the packet components and thus the different components experience dissipation at different times and rates. It is noted (not shown) that the vertical wavelength remains constant in time when the wave packet propagates through a nonviscous atmosphere; therefore, the shift from long to short dominant vertical wavelengths results from dissipation and not dispersion alone.

The evolution of the maximum energy density over time is shown in Figure 3, Case 1, panel (c) (for both viscous and inviscid propagation). There is a rapidly exponential decay from the onset as dispersion acts to spread the wave energy throughout the atmosphere. Both the viscous and nonviscous energy densities decay at the same rate until ~150 min, showing that the dispersion alone causes the reduction in amplitude up until that time. This has interesting implications for ray tracing, in particular, the wave action density which governs the amplitude of a ray (see Marks & Eckermann, 1995, section 2c). The ray trace formalism assumes conservative propagation (constant, density-scaled amplitude) along a ray unless acted upon by dissipation. However, Case 1, panel (c) shows that the amplitude of maximum energy density has decayed to 20% of its initial value through dispersion alone, before viscosity even has an impact. This highlights another difficultly in trying to use a single-ray approach to describe packets with strong dispersion. As described in Marks and Eckermann (1995), a ray tube formalism, or other more sophisticated methods are needed to accurately describe a dispersive packet, requiring a way for individual rays to *communicate* their amplitudes to each other to form a whole packet. Such a method is described in Vadas and Fritts (2009) who ray traced up to 2 million rays simultaneously. They consider the phases of those waves and reconstruct the gravity wave field with the use of momentum flux averaging and the gravity wave polarization relations to correct for amplitude decrease due to dispersion.

In contrast to Case 1, Case 2 is spectrally quasi-monochromatic and, as such, dispersion is relatively weak. Case 2, panel (a) shows that the packet remains fairly coherent with time until ~175 min, when dissipation shifts the central wavelength to lower values and the group velocity and energy density paths begin to diverge. Dissipation in this case acts more on the packet as a whole due to the relative lack of dispersion, and as such, the vertical wavelength only decreases by a kilometer (as seen in panel b). As a result of the relative lack of dispersion, the maximum energy density shown in Figure 3, Case 2, panel (c) declines much more gradually than Case 1, panel (c), but steepens significantly as dissipation begins to act on the packet in a significant way. Another effect of the narrowband nature is that the altitude the maximum energy density reaches is higher than that for the spectrally broad Case 1. Therefore, the path of the centrum of a wave packet, and its maximum energy density, evolve very different as a result of the bandwidth of the packet, even though the central wavelength, frequency, and launch altitude are the same. Bandwidth is a crucial parameter to consider

when describing the evolution of a wave packet. Despite the dispersion being relatively weak in Case 2, the amplitude of the maximum energy density still decreases linearly in time even when no viscosity is present (i.e., the red line in Figure 3, Case 2, panel c). Once again, typically, ray theory applied to a single ray alone would not account for this effect in the absence of dissipation.

Cases 3 and 4 are the same as Cases 1 and 2 except that they are launched from 80-km altitude rather than 40 km. This means that the packets have less time to disperse before viscosity acts to damp the wave packet. As a result, the group velocity and energy density paths diverge much earlier and also the energy density path reaches a higher altitude before ceasing upward propagation. The decrease in vertical wavelength becomes more dramatic in both Cases 3 and 4, panel (b), when compared to Cases 1 and 2, panel (b) and the maximum energy density decreases more rapidly than when compared to Cases 1 and 2, panel (c). Therefore, changing the launch altitude of a wave packet, with identical initial parameters, can also significantly alter the amplitude, altitude, and spectral evolution of the packet. This has implications for in situ and/or secondary wave generation in the MLT. If a wave spectrum is generated with the same wavelength and period in the troposphere, or in the mesosphere, we cannot assume their evolutions will be similar. Equally, the forcing they produce as a result of momentum flux deposition will be more localized and stronger if dispersion of the packet is minimized (either by having a higher launch altitude or having a more narrowband source).

It is noted that all of these cases show a spectral evolution as described by Heale et al. (2014), where the fast, long wavelength components are dissipated first causing the vertical wavelength to shift from large to small values as time progresses. Simulations are also run with $\lambda_x = 40$ km, $\lambda_z = 20$ km, launched from 40 km (figures not shown). These show the same effect as for the $\lambda_z = 10$ km cases but with a more rapidly decreasing vertical wavelength in time. This is because (1) dispersion causes the depth of the packet to become large over time, and as such, there is a considerable variation in the kinematic viscosity (ν) over the depth of the wave packet; (2) the packet propagates into the dissipative region rather than being generated in situ,; thus, the leading edge arrives at the viscous region first and experiences dissipation before the main body of the packet does. This effect was also seen in the ray trace studies of Vadas and Liu (2013) and Vadas et al. (2015), which required launching a large number of rays of different initial parameters and group velocities that describe the evolution of the packet spectrum. Using ray tracing to describe a packet with a single ray that propagates at the group velocity would not adequately describe the path, or evolution, of the packet.

4.2. Cases 5 and 6

Figure 4 shows the $\lambda_x = 40$ km, $\lambda_z = 5$ km cases launched from 80-km altitude, with Case 5 being the spectral broadband case (one vertical wavelength packet FWHM), and Case 6 being the quasi-monochromatic case (three vertical wavelength packet FWHM). While Cases 1–4 investigated how dissipation and dispersion were effected by launch altitude and bandwidth, Cases 5 and 6 consider the effect of an initial vertical scale that is smaller than the scale height of the atmosphere (smaller than the vertical scale of viscosity). This is an assumption which is central to the WKB approximation made by ray trace theory ($|m| \gg 1/2H$) and in Walterscheid (2013).

For Case 5, panel (a) where the packet is spectrally broad, significant dispersion occurs but far less so than when the initial vertical wavelength is 10 km (as in Case 3). This is because the range of group velocities associated with the 5-km packet are smaller than the 10-km one; thus, dispersion occurs at a slower rate. In addition, dissipation acts to damp the packet more rapidly for Case 5 than Case 3 (since the dissipation rate is great for smaller vertical wavelengths). In general, the rate of dispersion is a function of the bandwidth (thus the localization or impulsiveness) of the packet and the initial central vertical wavelength and phase speed. The dissipation rate, however, is a function of the vertical wavelength relative to the scale height of the atmosphere, since molecular kinematic viscosity is strongly influenced by the ambient density. Case 5, panel (b) follows the spectral evolution mechanism suggested in Heale et al. (2014) in which the vertical wavelength decreases in time and the energy density path diverges from the inviscid group velocity path as the longer vertical wavelength components are dissipated first. This happens in spite of the vertical scale being smaller than the atmospheric scale height, which was one of the conditions laid out in Walterscheid (2013) for the smaller wavelengths to be dissipated first and for the packet's central wavelengths to shift to larger values. This highlights the importance of considering dispersion and bandwidth when modeling/observing gravity wave packets. Case 6, where the packet is narrowband (thus weakly dispersive), and the central vertical wavelength is smaller than the scale height, fits the central assumptions for ray tracing. However, in order for the packet to be narrowband, the spatial localization of the packet has to incorporate several cycles of the wave

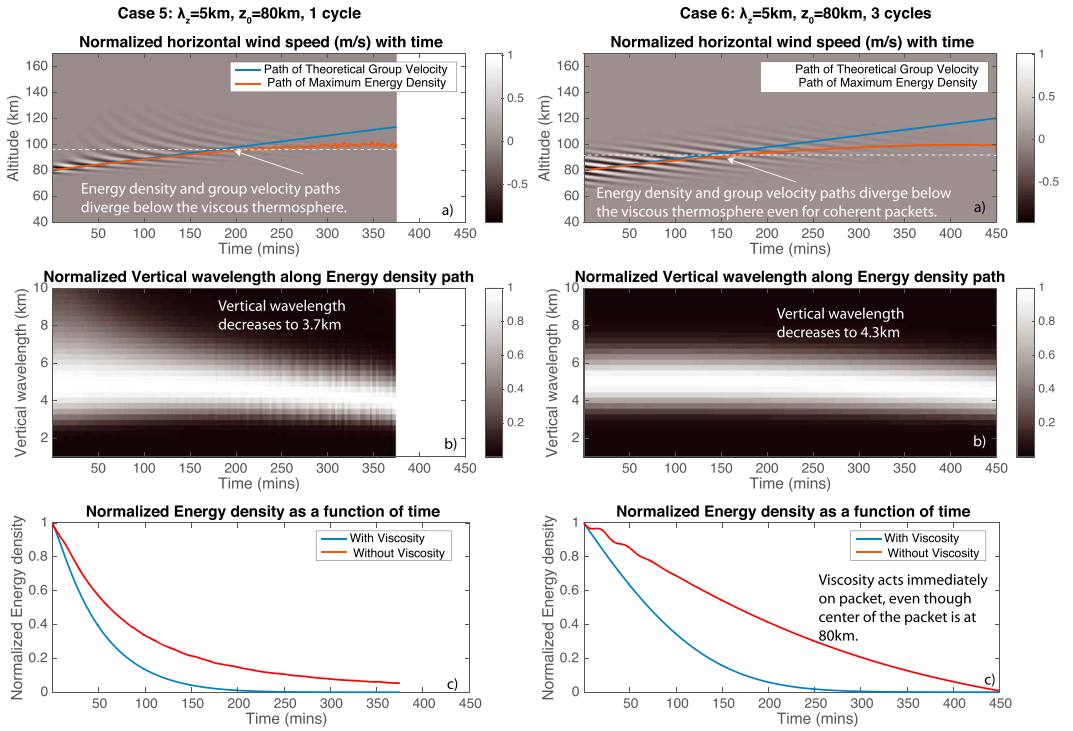

Figure 4. Simulation results for Cases 5 and 6 showing: (a) the scaled, normalized horizontal velocity as a function of time, with inviscid group velocity and maximum energy density paths overlaid, (b) the normalized vertical wavelength spectrum, and (c) the value of the maximum energy density with time for viscous and inviscid version of the simulation.

(via Fourier theory); for Case 6, this means that the vertical scale of the packet needs to be ~15 km (three vertical wavelengths), which is now greater than the scale height of the atmosphere. Therefore, the viscosity still varies meaningfully over the depth of the packet. As a result, the path of maximum energy density still diverges from the group velocity before the centrum of the packet reaches the thermosphere (divergence begins at about 85 km), suggesting that the leading edge of the packet (largest vertical wavelength and vertical group velocity) is still dissipating in advance of the rest of the packet. Case 6, panel (b), also indicates a shift in the central vertical wavelength to smaller values in time, albeit a small shift (from 5 to 4.3 km). Panel (c) in Figure 4, also indicates that dissipation due to viscosity acts on the packet very soon after launch since the maximum energy density in the inviscid (red) and viscous (blue) simulations diverge from each other very early in the simulation. The decrease in the inviscid maximum energy density in narrowband case highlights that dispersive amplitude decay occurs and needs to be accounted for, even for a narrowband packet whose central vertical wavelength is smaller that the scale height.

4.3. Cases 7–10

In Cases 7–10 (Figure 5), both the 5-km and 10-km vertical wavelength waves are launched at 120 km for both spectrally broadband and narrowband initializations. As such, the packets originate in a region where the molecular viscosity and thermal conductivity are nonnegligible and dissipation will act on the packet from the outset rather than having a wave packet propagate into the dissipative region. In reality, waves originating in this region are likely secondary waves caused by dissipation of a primary gravity wave packet (Vadas & Liu, 2009, 2013) or through breaking and instability (Bossert et al., 2017; Lund & Fritts, 2012). The scales and periods of these secondary waves in the former case are dependent upon the time and spatial scales of the body forcing created by the dissipating primary wave (e.g., Vadas & Liu, 2009, 2013).

Figure 5, Case 7 shows the 5-km vertical wavelength wave packet, that is spectral broad (spatially localized). This is the first case that shows a maximum energy density path that reaches higher altitudes than the group velocity path (panel a), and a spectrum that evolves from smaller to longer vertical wavelengths in time (panel b). This is due to three main factors: First, the vertical wavelength is smaller than the scale height. Second, the packet is initially very localized, meaning that the viscosity remains fairly constant over the packet depth. Third, (and crucially), the packet is launched in the viscous region, so dissipation acts immediately on the

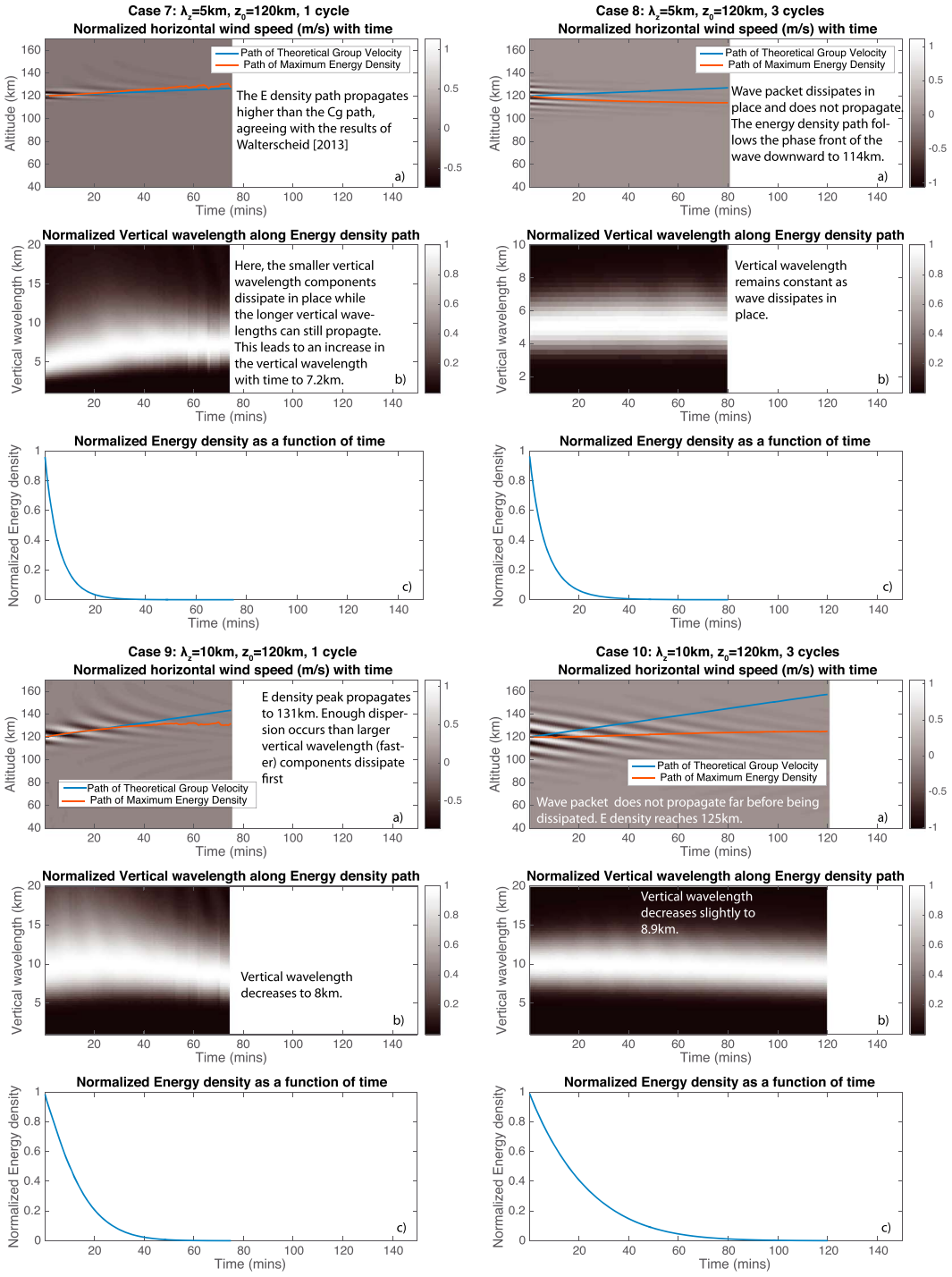

Figure 5. Simulation results for Cases 7–10 showing (a) the scaled, normalized horizontal velocity as a function of time, with inviscid group velocity and maximum energy density paths overlaid, (b) the normalized vertical wavelength spectrum, and (c) the value of the maximum energy density with time.

whole packet. Combined, this leads to a spectral and path evolution as described in Walterscheid (2013). The viscosity preferentially and immediately acts to damp the small scales, removing them from the packet and leaving the larger scale to propagate for a short time before they too are dissipated. The whole packet is dissipated very quickly and the maximum energy density decays to near zero after just 30 min (panel c).

Case 8 shows the 5-km vertical wavelength wave packet, when the wave packet is narrowband. Since the spectral content of this packet is much more narrow than Case 7, it contains a lesser abundance of longer

wavelengths that would decay more slowly and could propagate to higher altitudes. As a result, the entire packet dissipates in place without propagating upward at all. In fact, the energy density path moves downward in time, because the viscosity varies over the depth of the packet and the lower portions of the packet decay at a marginally slower rate than the top. The central vertical wavelength remains constant in time for this case.

For Case 9 (10 km, broadband packet), the dominant vertical wavelength first increases slightly and then decreases. Early-on scale-dependent dissipation dominates (as in Case 7); but, as the wave packet disperses, the selective removal of the long wavelengths dominates. For Case 10 (10 km, narrowband packet), the evolution is similar to Case 8; however, this packet dissipates at a slower rate and can propagate upward for a short distance. This is because the packet depth spans a greater depth that in Case 8 (thus, the lower part is generated in a less viscous region) and the central vertical wavelength is larger and so dissipation due to viscosity is less rapid.

There are two implications that arise for secondary waves generated in the thermosphere from these cases. First, if coherent, narrowband, secondary wave packets generated in the thermosphere are going to be able to survive and propagate, they need to have large vertical wavelengths and high phase speeds (Vadas, 2007). Second, if a wave packet with a central wavelength smaller than the local scale height is going to exist for any significant length of time, it will need to have sufficiently broad spectra (that contain waves with large vertical scales and phase speeds that can survive). From these simulations, wave packets with parameters that fulfill the assumptions, and follow the evolution, laid out in Walterscheid (2013) (i.e., evolve from shorter to longer vertical wavelengths) appear most likely to be secondary waves generated in the thermosphere and not primary waves. However, secondary waves that fulfill these assumptions (coherent packets, with vertical scales smaller than the scale height) are also likely to decay rapidly in the thermosphere unless they have broad spectra. Therefore, it is unlikely to observe such waves in the thermosphere. Waves observed in the thermosphere typically have very large vertical scales and high phase speeds (Vadas, 2007; Vadas & Liu, 2013). The need to accurately account for dispersion is necessary to capture the evolution of the wave packet spectra from longer to shorter vertical wavelengths if the wave is launched in the lower/middle atmosphere but is also needed to account for the evolution from shorter to longer wavelengths that can occur when waves are launched in the dissipative thermosphere. It is likely that waves commonly observed in the thermosphere are either secondary waves generated in the MLT or thermosphere with large vertical wavelengths and horizontal phase speeds, or the high-frequency, large vertical wavelength components of a primary wave packet propagating up from their source in the lower atmosphere (i.e., Vadas et al., 2003; Vadas & Fritts, 2005; Vadas & Liu, 2009).

The results are summarized for Cases 1–10 in Table 2.

It is key to note that the vertical wavelength plots in Cases 1–10 were normalized in the figures for clearer presentation, as amplitudes become small; however, this can be visually misleading as it obscures the mechanism that causes the decrease in the central vertical wavelength. Figure 6 shows the same vertical wavelength figures presented in Cases 3–6, but without normalization. It is clear from these figures that the spectrum tapers from the long vertical wavelength edge of the spectrum, since the waves that propagate fastest also dissipate sooner in the thermosphere. This leads to the evolution in the central vertical wavelength to smaller values (blue lines in Figure 6) as a result of the eroding of long vertical wavelength components. The evolution of the spectrum is thus the result of removal of long wavelength components rather than a shifting or refracting individual components within the spectrum, the latter being an incorrect conclusion that one may draw from inspection of the normalized vertical wavelength plots alone (Heale et al., 2014).

4.4. Inviscid Energy Density Evolution

The formal solution, for example, for the horizontal wind described by a wave equation is

$$u(z,t) = \frac{1}{\sqrt{2\pi}} \int_{-\infty}^{\infty} A(m) e^{(i(mz-\omega(m)t)} \mathrm{d}m \tag{8}$$

where from Walterscheid (2013),

$$A(m) = \frac{1}{2\sqrt{2\pi}} \int_{-\infty}^{\infty} \left[u(z,0) + \frac{i}{\omega(m)} \frac{\partial u}{\partial t}(z,0) \right] e^{-imz} \mathrm{d}z \tag{9}$$

Table 2
Summarized Results of Cases 1–10

Case	Initial λ_z (km)	Final λ_z (km)	Change (%)	Launch z (km)	Final z (km)	Initial width (λ_zs)	Summary
1	10	6.3	−37	40	104	1	Significant dispersion occurs and dissipation acts on fast, large λ_z components first.
2	10	8.9	−10.8	40	117	3	Packet remains fairly coherent, minimal dispersion.
2	10	8.9	−10.8	40	117	3	Packet remains fairly coherent, minimal dispersion.
3	10	6.6	−34	80	115	1	Higher launch z means less time to disperse before dissipation occurs.
4	10	8.9	−10.8	80	121	3	Similar to Case 2.
5	5	4	−20	80	100	1	Dispersion not as great as Case 3, due to smaller initial λ_z.
6	5	4.6	−8.4	80	100	3	Packet remains coherent, little change in λ_z.
7	5	7.2	44.6	120	129	1	λ_z increases due to scale-dependent removal of short wavelength components.
8	5	5.5	9.8	120	120	3	Packet dissipates in place without dispersion or any upward propagation.
9	10	8.6	−13.6	120	133	1	Fairly rapid dissipation, but some dispersion still occurs.
10	10	8.9	−10.7	120	125	3	Dissipation occurs quickly with virtually no dispersion.

Note. Note that 8 out of the 10 cases show an increase in the central vertical wavelength over time due to dispersion causing the faster longer vertical wavelengths to be removed first, while only two show an increase in the vertical wavelength due to scale-dependent dissipation removing the shorter wavelengths first.

For simplicity, we ignore the initial tendency and assume an initial Gaussian disturbance of the form

$$u(z,0) = U\exp(-z^2/2\sigma_{z_0}^2)e^{im_0 z} \tag{10}$$

The initial spectrum (10) is given via a Fourier transform as

$$A(m) = \frac{1}{2}U\sigma_{z_0}e^{-\frac{1}{2}(m-m_0)^2\sigma_{z_0}^2} \tag{11}$$

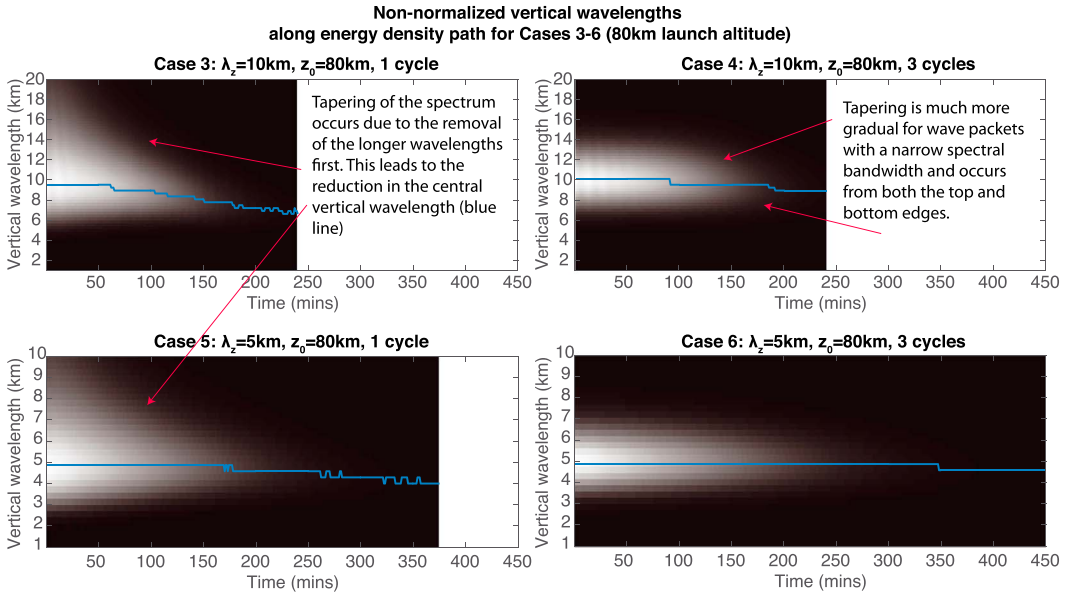

Figure 6. The nonnormalized vertical wavelength plots as a function of time for Cases 3–6. The blue line represents the central (dominant) vertical wavelength. The figure shows that the *migration* in the central vertical wavelength is a result of the removal of the longer vertical wavelengths in time caused by dissipation, that is, and is not due to shifting or refraction of the spectrum to shorter wavelengths.

This illustrates the inverse relationship between the spatial localization σ_{z_0} and the spectral width $1/\sigma_{z_0}$. The time evolution of the packet is then given by

$$f(z,t) = \int_{-\infty}^{\infty} \exp(i(mz - \omega(m)t)\tilde{f}(m)\mathrm{d}m \tag{12}$$

In order to obtain an approximate solution, the dispersion relation $\omega(m)$ is Taylor expanded about the central wave number m_0 to second order, under the assumption that the spectrum is sharply peaked about the central wave number :

$$\omega(m) = \omega(m_0) + (m - m_0)\frac{\partial\omega}{\partial m} + \frac{1}{2}(m - m_0)\frac{\partial^2\omega}{\partial m^2} \tag{13}$$

The first-order term gives the vertical group velocity ($C_g = \frac{\partial\omega}{\partial m}$), and the second-order term $\Gamma = \frac{\partial^2\omega}{\partial m^2}$ is a measure of the spreading of the packet (both are assumed constant). The integral (8) now becomes

$$u(z,t) = \frac{U}{2\sqrt{2\pi}}\int_{-\infty}^{\infty}\sigma_z \exp\left[-\frac{1}{2}(m - m_o)^2\sigma_z^2\right]\exp i\left[mz - \left(\omega_o + C_g(m - m_o) + \frac{1}{2}\Gamma(m - m_0)^2\right)t\right]\mathrm{d}m \tag{14}$$

The solution is

$$u(z,t) = \frac{U}{2}\frac{1}{[1 + i\Gamma t/\sigma_z^2]^{1/2}}\exp\left[-\frac{(z - C_g t)^2}{2\sigma_z^2(1 + i\Gamma t/\sigma_z^2)}\right]\exp i(m_0 z - \omega_0 t) \tag{15}$$

whence

$$|u(z,t)|^2 \propto \frac{\sigma_z}{\sigma_z(t)}\exp\left[-\frac{(z - C_g t)^2}{\sigma_z^2(t)}\right] \tag{16}$$

where $\sigma_z(t) = \sigma_z(0)\sqrt{1 + \frac{\Gamma^2}{\sigma_z^4(0)}t^2}$. The solution takes the form of a Gaussian-enveloped packet that propagates at the group velocity C_g and spreads and decreases in amplitude with time as $\sigma_z(t)$ increases. Note that while these results are for inviscid propagation, the molecular viscosity ν enters the Fourier integral as $\exp(-\nu m^2 t)$. Therefore, the expression can be combined with that of Γ to give $\exp[-(\nu + \frac{1}{2}\Gamma)m^2 t]$ and the time-dependent width can be written as $\sigma_z(t) = \sigma_z\sqrt{1 + \frac{(2\nu+\Gamma)^2}{\sigma_z^4}t^2}$.

Figure 7 shows the evolution of the energy density in an inviscid atmosphere for Cases 1 and 2, with the upper panels (a) and (c) showing the time evolution with the maximum energy density path, and theoretical group velocity paths overlaid. The lower panels (b) and (d) show the energy density with altitude at four discrete times.

For Case 1 (the broadband case), it is very clear that the initial Gaussian shape evolves into an asymmetric form as the faster, longer wavelength components propagate ahead of the main bulk of the packet. Over time, this leads the maximum energy density path to lag slightly behind the group velocity path. The simulation then, is at odds with the theoretical description for a dispersive wave packet, which assumes that the packet remains Gaussian over time and does not account for the asymmetric evolution. For Case 2 (the narrowband case), the packet does, however, remain Gaussian due to its relatively narrow spectrum (see below). The Gaussian increases in width and decreases in amplitude over time, as suggested by the analytical solution. However, the maximum energy density path advances slightly quicker than the theoretical group velocity path.

One of the assumptions made in the analytical description of wave packet evolution is that the wave spectrum is sharply peaked around the central wave number (in this case m_0; Jackson, 1975; Walterscheid, 2013; Walterscheid & Hecht, 2003), which allows for the Taylor expansion of the dispersion relation and leads to packet propagation at the group velocity. The validity of this assumption for a given packet was suggested by Walterscheid (2013) to be given by the ratio of the second derivative of ω (Γ) times the initial value of σ_z^{-1} (the measure of the dispersion in group velocity) to the first derivative of ω (C_g). Here we modify that slightly to be ratio of the quadratic term in the Taylor expansion (the dispersive term) times σ_z^{-1} to the linear term (the group velocity term) and use the anelastic rather than the Boussinesq dispersion relation (neglecting the Coriolis parameter):

$$\gamma = |\frac{1}{2\sigma_z}\Gamma/C_g| \tag{17}$$

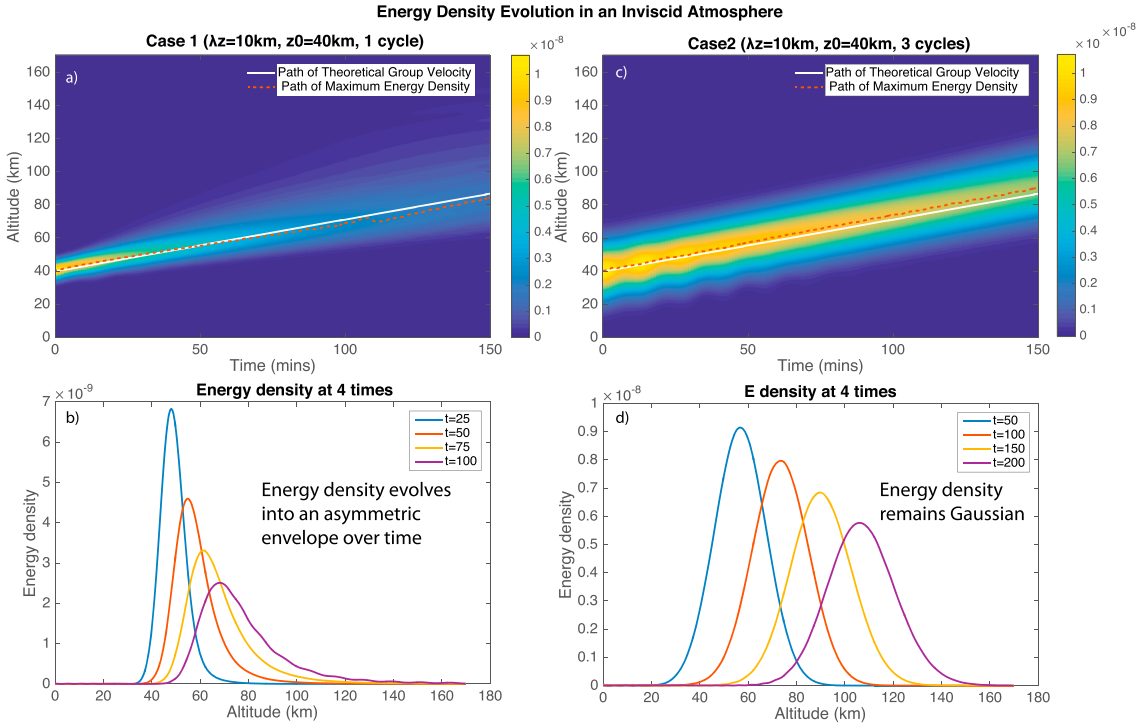

Figure 7. The energy density evolution for Cases 1 (a and b) and 2 (c and d), propagating through an inviscid atmosphere. The white (solid) and red (dashed) lines in panels (a) and (c) represent the group velocity path and path of maximum energy density, respectively.

whence,

$$\gamma = \left| \frac{1}{2m_0\sigma_z} \frac{2m_0^2 - k^2 - 1/4H^2}{k^2 + m_0^2 + 1/4H^2} \right| \tag{18}$$

Values of γ should be less than order unity for the propagation of the wave packet to be given by C_g (neither too broad nor too dispersive). For the parameters of Cases 1 and 2, γ has values of 0.4 and 0.17, respectively. Thus, Cases 1 and 2 meet this criterion. In the limit of large m^2 (quasi-hydrostatic Boussinesq) the dispersion relation is

$$\omega = \frac{N^2 k}{m} \tag{19}$$

and gives the result

$$\frac{\partial^n \omega}{\partial m^n} = (-1)^n n! \frac{\omega}{m^n} \tag{20}$$

When this is inserted in the Taylor expansion for ω this becomes

$$\omega = \omega_0 - \frac{\Delta m}{m_0} + \left(\frac{\Delta m}{m_0}\right)^2 - \left(\frac{\Delta m}{m_0}\right)^3 + \ldots \tag{21}$$

For a broadband disturbance $\Delta m \sim m_0$ (21) is a very slowly converging series. The first three terms describe the propagation and spreading of a Gaussian wave packet. The fourth term and higher contribute to non-Gaussian behavior. Typical gravity waves are not too far from hydrostatic Boussinesq waves. For these waves the evolution of broadband wave packets is not well described by the standard theory. To accurately account for the whole spectrum in a broadband case, a numerical solution to equations (8) and (9) would likely be needed, integrating over the full dispersion relation; or by direct numerical solution, as done here. Note that when $m_0^2 \sim \frac{1}{2}(k^2 + 1/4H^2)$, the minimum of equation (18), waves are minimally dispersive.

4.5. Viscous Energy Density Evolution

Figure 8 shows the same plots as Figure 7 but for propagation through a viscous atmosphere. When comparing the two, it is easy to see how the leading edge of the packet is dissipated first, removing the faster, longer

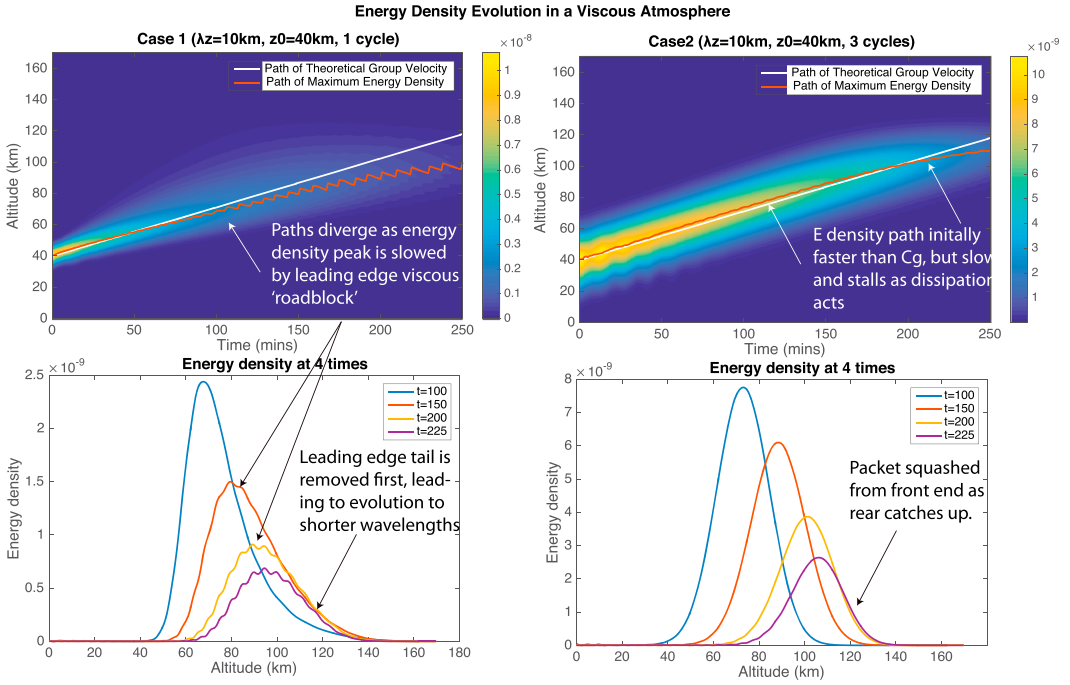

Figure 8. The energy density evolution for Cases 1 (a and b) and 2 (c and d), propagating through a viscous atmosphere. The white and red lines in panels (a) and (c) represent the group velocity path and path of maximum energy density, respectively.

wavelength components first. In Case 1 (panels a and b), it is the long tail of the spectrum that was seen in the inviscid cases, that gets truncated from the packet first. As a result, the packets' dominant vertical wavelength evolves from longer to shorter values as time progresses. It is also clear to see how the peak in the energy density distribution stalls in its upward motion as the leading edge of the packet is dissipated. The packet hits a vertical *roadblock* diminishing the amplitude from the leading edge while the center and rear of the packet catch up. It is this effect that leads to the divergence between the path of the maximum energy density and inviscid group velocity once dissipation acts on the packet.

4.6. Cases 11–14

Previous studies (e.g., Fritts & Vadas, 2008; Vadas, 2007; Vadas & Fritts, 2006; Yiğit & Medvedev, 2010) have investigated the effects of different thermospheric temperature structures, related to solar activity, on gravity wave dissipation. They found that in high solar activity, waves experience less vertical damping and favorable propagation to higher altitudes due to effective expansion of the atmosphere and thus less rapidly increasing viscosity with altitude. As a result, the maxima of gravity wave momentum deposition occur much higher under stronger solar conditions but at weaker amplitudes.

Cases 11–14 (Figure 9) show the 5-km and 10-km vertical wavelength packets, launched from $z = 40$-km altitude, propagating through the realistic thermospheric temperature structure. The realistic thermosphere adds two noticeable effects: (1) The thermospheric temperature profile refracts the waves, in turn altering the vertical propagation of the packet (i.e., Vadas & Fritts, 2006) and (2) affects the variation in molecular viscosity as a result of the changing scale height H. The blue curves in panel (a) show the inviscid group velocity paths for the central wave number of the packet. The orange curves in the (b) panels show the vertical wavelengths inferred from the adiabatic dispersion relation along the path of maximum energy density (red curve in panel a) assuming no dispersion.

In Case 11 ($\lambda_z = 5$ km, one cycle) panel (a), the packet disperses rapidly in time and by $t = 200$ mins, spans an altitude of ~130 km. The temperature gradient in the thermosphere leads to an increase in N^2, which refracts waves to larger vertical wavelengths, in turn, increasing their vertical group velocity. This increases the amount of dispersion relative to the isothermal cases as the leading edge of the packet, which reaches the thermospheric temperature gradient first, is accelerated away from the center of the packet even more. The same result is true for the 10-km vertical wavelength case (Case 13, panel a), except that the rate of dispersion

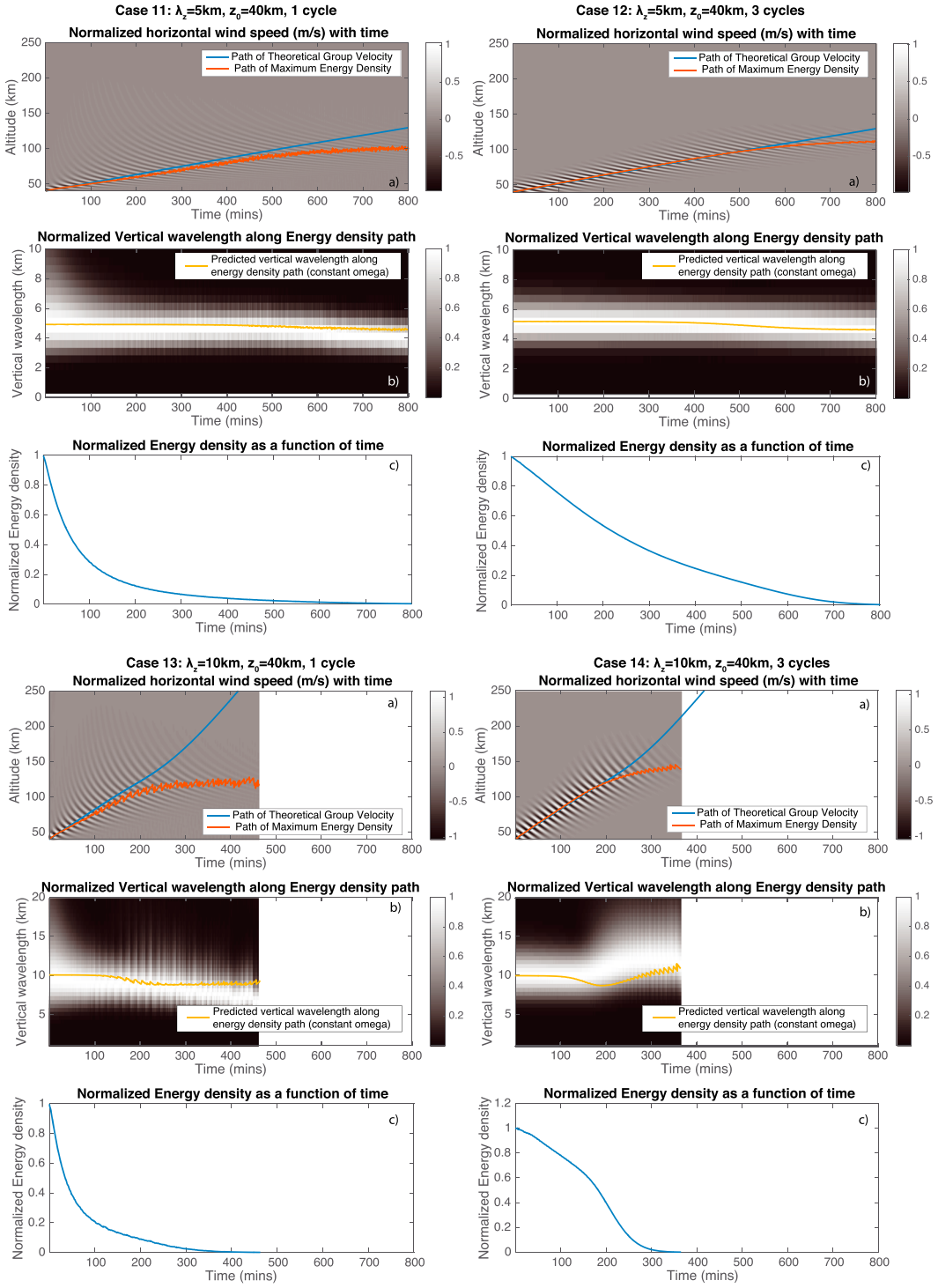

Figure 9. Simulation results for Cases 11–14 showing (a) the scaled, normalized horizontal velocity as a function of time, with inviscid group velocity and maximum energy density paths overlaid, (b) the normalized vertical wavelength spectrum, with the predicted vertical wavelength along the maximum energy density path shown in orange, and (c) the value of the maximum energy density with time. These are the cases of waves propagating through a realistic thermosphere.

Table 3
Summarized Results of Cases 11 – 14

Case	Initial λ_z (km)	Final λ_z (km)	Change (%)	Launch z (km)	Final z (km)	Initial width (λ_zs)	Summary
11	5	4.1	−18	40	99.5	1	Significant dispersion occurs, energy density path does not reach refracting portion of thermosphere.
12	5	4.6	−8	40	111	3	Weak dispersion leads to higher final energy density altitude than Case 11, but still does not reach refracting portion of thermosphere.
13	10	7.2	−28	40	120	1	Considerable dispersion occurs leading to reduction in central λ_z through dissipation of longer, faster components.
14	10	11.8	18	40	140	3	Packet remains coherent until thermosphere, central vertical wavelength refracted to larger λ_z by thermospheric temperature change.

Note. Due to dispersion, the energy density path does not penetrate high enough in the thermosphere for the background temperature change to significantly refract the central vertical wavelength for Cases 11 – 13 but has a noticeable effect in Case 14.

relative to the group velocity is smaller in this case. As with the isothermal cases, the path of maximum energy density path diverges from the inviscid group velocity path below the viscous thermosphere, suggesting that dissipation of the leading edge has a strong influence on the perceived path of the center of the packet and that the rate of dispersion has a significant influence on this evolution. This has interesting consequences for observations of waves generated by broadband packets. Instruments independently measuring wave activity in the mesosphere and thermosphere would infer different wave parameters in the two regions and may conclude that there are in fact two distinct waves present. However, these would be part of the same source and part of a single packet that could be measured across the stratosphere, mesosphere, and thermosphere simultaneously. The central vertical wavelength, in both Cases 11 and 13, evolve to shorter values in time.

For Cases 12 and 14 (the narrowband cases), the difference in the central vertical wavelength of the packets and their respective widths lead to significantly different evolutions. For the 5-km central vertical wavelength case (Case 12), the packet remains coherent throughout its propagation and the packet dissipates, together, rapidly as it enters the lower thermosphere. This is because the packet has a small central vertical wavelength (relative to the scale height), such that viscosity damps the packet more rapidly than the 10-km case. Also, the depth of the packet is comparable to the scale height; thus, the viscosity does not vary too much over the depth of the packet, so it dissipates at nearly equal rates across the packet. As a result the vertical wavelength decreases by only 0.4 km. For Case 14, the packet remains coherent enough, and the central vertical wavelength is large enough that path of maximum energy density penetrates into the lower thermosphere and is refracted to larger vertical wavelengths by the temperature gradient (Case can be seen in Case 14, panel b). When comparing with the equivalent isothermal case (Case 2), the decrease in the central vertical wavelength caused by dissipation is obfuscated by the refractive increase in vertical wavelength by the thermosphere. The dispersion, as noted for the broad band cases, is accelerated by the refractive effects of the thermosphere and the depth of the packet broadens significantly once the packet reaches the thermosphere (after ∼150 mins).

It is clear from these cases that the realistic thermospheric temperature can complicate the interpretation of gravity wave spectral evolutions. If the initial spectra are broad, or the vertical wavelength too short, then the maximum energy density path may not reach the region of the thermosphere where the temperature change has an effect on the evolution of the wave spectra. However, if the packet is relatively narrowband, and the central vertical wavelength is long enough, then the wave's maximum energy density path can penetrate into the thermosphere and the thermospheric temperature structure can change the evolution of the packets vertical wavelength. In addition, the refractive effect of the thermosphere (especially on the fast packet components) can act to accelerate dispersion and broaden the spatial extent of the packet. The results from Cases 11 – 14 are summarized in Table 3.

5. Discussion and Conclusions

In this paper, the relative effects of dispersion and dissipation of transient gravity wave packets of different spatial localizations (and thus spectral content) are explored. Numerical simulations were run with initial wave packet spans of one vertical wavelength (broadband), and three vertical wavelengths (narrowband) for packets with central vertical wavelengths of 5 km and 10 km. These packets were launched from 40, 80, and 120 km in order to control the amount of packet dispersion that occurs before dissipation becomes important. In order to delineate the effects of dispersion and dissipation, runs were also performed in an atmosphere that was free of viscosity.

Two specific spectral evolutions have been presented for linear transient wave packets and the aim was to test the limits of these two regimes. Theory states that viscosity and conduction will act to preferentially dissipate smaller scales given a spectrum of waves at the same altitude and, as such, Walterscheid (2013) predicted that broadband wave packets with a central vertical wavelength less than the scale height would evolve to longer vertical wavelengths under strong dissipation. Other studies, such as Heale et al. (2014), Liu et al. (2013), Vadas and Fritts (2005), and Vadas and Liu (2013), found that wave packets tended to evolve to smaller vertical wavelengths under dissipation.

We find that in all isothermal cases launched where the wave is essentially dissipation free (i.e., not in the thermosphere), dispersion is significant enough that the faster, longer vertical wavelength components reach the dissipative thermosphere first and are removed from the spectrum first, leading to the shorter, slower components to be dominant at later times. This was the mechanism laid out in Heale et al. (2014) and the spectrum evolves from its central vertical wavelength to smaller vertical wavelengths as time progresses. The effect is more dramatic for spectrally broad packets and small for the narrowband packets. It is noted, that this spectral evolution is solely the result of dissipation; the central vertical wavelength of the same wave, propagating in a nonviscous atmosphere, remains constant (as long as it remains linear). These cases are especially applicable to convective sources that produce a broad spectra of waves. It has also been shown that the spectrum of secondary waves created by dissipating primary wave can be broad in nature (Vadas et al., 2003). It is likely that packets generated by convective sources will evolve, in the manner described, from longer to shorter wavelengths and was seen to be prominent in studies assessing the impact of convectively generated waves on the thermosphere (Vadas & Liu, 2013; Vadas, 2013). It is also key to note that the dispersion, spectral evolution, and dissipation of these wave packets are highly time dependent. Most gravity wave parameterization schemes that include the effects of molecular viscosity assume a steady state solution, therefore, they will not accurately capture the inherently time-dependent dispersive effects of spectrally broad packets. Broadband packets will tend to deposit their momentum over a larger altitude depth and longer time scales than a quasi-monochromatic wave packet.

The results for spectrally broad packets also have implications for ray tracing applications. It was found that the path of maximum energy density diverges from the inviscid group velocity path far before either path reaches the viscous thermosphere region. This is because the leading edge of the packet, which contains the larger vertical wavelength spectral components, is subject to dissipation in the thermosphere first, thus reshaping the packet. An individual ray, used to represent an entire spectrum, would not experience a path deflection (in a windless, isothermal atmosphere) until acted upon by viscosity (e.g., Vadas & Fritts, 2005; Walterscheid, 2013). Equally, the amplitude of the maximum energy density decreases significantly due to dispersion alone. Once again, tracing a single ray typically considers conservative propagation and would not indicate a decrease in amplitude unless acted upon by viscous forces. Even for cases where the packet was relatively narrowband, dispersion still played a role in the decrease in amplitude of the maximum energy density. This suggests that ray trace simulations need to carefully consider the spectral bandwidth of the packet and likely requires an approach to ray tracing that includes a multiplicity of rays that reproduce the spectral content of a wave packet A(k) in order to properly account for dispersion in wave packets and the resulting amplitude decay. A technique to properly account for dispersion in ray tracing is presented in Vadas and Fritts (2009). In addition, analytical approaches suggest that an initial Gaussian packet should evolve as a Gaussian over time, whose width increases and amplitude decreases. However, energy density model results suggest that the broadband wave packets can evolve into asymmetric distributions, which are elongated by the fast, long wavelength packet components accelerating in front of the bulk of the packet. This effect is most pronounced for broadband waves with $m^2 \gg k^2$. For such broadband packets, wave solutions should

be constructed by full integration over the spectral space rather than expanding the dispersion relation to the first or second order, or by direct numerical simulations.

If the packet has a central vertical scale smaller than the atmospheric scale height, is sufficiently broadband, and crucially, is launched in the thermosphere (as, say, by secondary wave generation), then the scale-dependent dissipation acts to remove the smaller vertical wavelengths first, and the dominant wavelength shifts to longer values as described in Walterscheid (2013). Even so, these packets are relatively short-lived unless the spectra are very broad and contain packet components with vertical wavelengths much larger than the scale height (Vadas, 2007). If the packet is spectrally narrowband, the waves dissipate rapidly in place with little to no upward propagation and the vertical wavelength remains approximately constant as the entire spectra is dissipated together. This suggests that waves observed in the thermosphere are either the large vertical wavelength, high phase speed components of packets launched in the lower/middle atmosphere, or secondary waves generated in situ that necessarily have vertical wavelengths greater than the scale height (or high phase velocities), or are generated as spectral broad packets by impulsive, or very localized forcing. The wave field in the upper atmosphere comprises a superposition of coherent wave packets and a continuum. Our results indicate that broadband disturbances launched in the lower atmosphere are strongly dispersed by the time they reach the upper atmosphere; this suggests that a significant source for the continuum, if the not main one, is fully dispersed wave packets.

Thermosphere temperature gradients can exacerbate the level of dispersion by refracting the faster, long vertical wavelength components of a packet to even faster vertical group velocities, accelerating the spreading of the packet over altitude. If the wave packet has a large enough central vertical wavelength that it can penetrate into the section of the thermosphere where the temperature gradient becomes significant, then the spectral evolution can be dominated by the refraction to larger vertical wavelengths which can obfuscate the decrease in vertical wavelength caused by dissipation.

If the energy density path of a wave propagates into regions of the thermosphere where the temperature changes significantly, changes in the rate of viscous dissipation and vertical wavelength due to thermal structure can affect the dominant vertical wavelength. For the 5-km narrow and broadband cases and the 10-km broadband case, the wavelengths inferred from the wavelet analysis are shorter than the adiabatic wavelengths after the group and maximum energy paths diverge by a significant amount. This is consistent with the combined effects of dispersion and the preferential absorption of the long fast waves, as for the isothermal case, but the divergence takes place later and the magnitude of the effect is less. For the 10-km narrowband case, however, the inferred wavelength becomes significantly larger after the paths diverge. This occurs because the packet remains coherent until the main part of the packet reaches the lower thermosphere where it dissipates by means of scale selective viscous dissipation.

The localization, and thus spectral content, of a wave packet is a crucial parameter in determining its amplitude and spectral evolution. The effect of dispersion on the amplitude decrease of a wave packet is somewhat underappreciated and should be carefully considered for ray tracing applications to inherently broad spectra, such as those generated by convection. Equally, results suggest that the central vertical wavelength of most transient packets will evolve from longer to shorter wavelengths in time under dissipation. Packets that evolve to longer vertical wavelengths as a result of dissipation are likely secondary waves generated in situ in the thermosphere.

Acknowledgments

Research by C. J. Heale and J. B. Snively was supported under NSF grants AGS-1151746 and AGS-1344356. R. L. Walterscheid was supported by NSF grant AGS-1344350. The authors would like to thank the Editors and three anonymous reviewers for their valuable contributions to this manuscript. Text files needed to reproduce the figures in this paper are provided in the supporting information.

References

Alexander, M. J., & Rosenlof, K. H. (1996). Nonstationary gravity wave forcing of the stratospheric zonal mean wind. *Journal of Geophysical Research*, *101*(D18), 23,465–23,474. https://doi.org/10.1029/96JD02197

Baldwin, M. P., Gray, L. J., Dunkerton, T. J., Hamilton, K., Haynes, P. H., Randel, W. J., et al. (2001). The quasi-biennial oscillation. *Reviews of Geophysics*, *39*(2), 179–229. https://doi.org/10.1029/1999RG000073

Bale, D. S., LeVeque, R. J., Mitran, S., & Rossmanith, J. A. (2002). A wave propagation method for conservation laws and balance laws with spatially varying flux functions. *Journal of Scientific Computing*, *24*(3), 955–978.

Bossert, K., Kruse, C. G., Heale, C. J., Fritts, D. C., Williams, B. P., Snively, J. B., et al. (2017). Secondary gravity wave generation over New Zealand during the deepwave campaign. *Journal of Geophysical Research: Atmospheres*, *122*, 7,834–7,850. https://doi.org/10.1002/2016JD026079

Djuth, F. T., Sulzer, M. P., Gonzeles, S. A., Mathews, J. D., Elder, J. H., & Walterscheid, R. L. (2004). A continuum of gravity waves in the Arecibo thermosphere. *Geophysical Research Letters*, *31*, L16801. https://doi.org/10.1029/2003GL019376

Fritts, D., & Alexander, M. J. (2003). Gravity wave dynamics and effects in the middle atmosphere. *Reviews of Geophysics*, *41*(1), 1003. https://doi.org/10.1029/2001RG000106

Fritts, D. C., & Lund, T. S. (2011). Gravity wave influences in the thermosphere and ionosphere: Observations and recent modeling, *Aeronomy of the Earth's Atmosphere and Ionosphere* (pp. 109–130). Netherlands: Springer.

Fritts, D. C., & Vadas, S. L. (2008). Gravity wave penetration into the thermosphere: Sensitivity to solar cycle variations and mean winds. *Annales Geophysicae*, *26*(12), 3,841–3,861. https://doi.org/10.5194/angeo-26-3841-2008

Garcia, R. R., & Solomon, S. (1985). The effect of breaking gravity waves on the dynamics and chemical composition of the mesosphere and lower thermosphere. *Journal of Geophysical Research*, *90*, 3,850–3,868.

Heale, C. J., Bossert, K., Snively, J. B., Fritts, D. C., Pautet, P.-D., & Taylor, M. J. (2017). Numerical modeling of a multiscale gravity wave event and its airglow signatures over Mount Cook, New Zealand, during the deepwave campaign. *Journal of Geophysical Research: Atmospheres*, *122*, 846–860. https://doi.org/10.1002/2016JD025700

Heale, C. J., Snively, J. B., Hickey, M. P., & Ali, C. J. (2014). Thermospheric dissipation of upward propagating gravity wave packets. *Journal of Geophysical Research: Space Physics*, *119*, 3,857–3,872. https://doi.org/10.1002/2013JA019387

Hickey, M. P., Taylor, M. J., Gardner, C. S., & Gibbons, C. R. (1998). Full-wave modeling of small-scale gravity waves using airborne lidar and observations of the Hawaiian airglow (ALOHA-93) O(1S) images and coincident Na wind/temperature lidar measurements. *Journal of Geophysical Research*, *103*(D6), 6,439–6,453.

Hocke, K., & Tsuda, T. (2001). Gravity waves and ionospheric irregularities over tropical convection zones observed by GPS/MET radio occultation. *Geophysical Research Letters*, *28*, 2,815–2,818.

Holton, J. (1982). The role of gravity wave induced drag and diffusion in the momentum budget of the mesosphere. *Journal of the Atmospheric Sciences*, *39*, 791–799.

Holton, J. R. (1983). The influence of gravity wave breaking on the general circulation of the middle atmosphere. *Journal of the Atmospheric Sciences*, *40*, 2,497–2,507.

Holton, J. R., & Alexander, M. J. (2000). The role of waves in the transport circulation of the middle atmosphere. In D. E. Siskind, S. D. Eckermann, & M. E. Summers (Eds.), *Atmospheric science across the stratopause* (Vol. 123, pp. 21–35). Washington, DC: AGU.

Hung, R. J., & Kuo, J. P. (1978). Ionospheric observations of gravity-waves associated with Hurricane Eloise. *Journal of Geophysical Research*, *45*, 67–80.

Jackson, J. D. (1975). *Classical Dynamics*. New York: Wiley-Interscience.

LeVeque, R. J. (2002). *Finite Volume Methods for Hyperbolic Problems*. Cambridge: Cambridge University Press.

Lighthill, M. J. (1965). Group velocity. *IMA Journal of Applied Mathematics*, *1*(1), 1–28.

Lindzen, R. S. (1981). Turbulence and stress owing gravity wave and tidal breakdown. *Journal of Geophysical Research*, *86*(C10), 9,707–9,714.

Liu, X., Xu, J., Yue, J., & Vadas, S. L. (2013). Numerical modeling study of the momentum deposition of small amplitude gravity waves in the thermosphere. *Annales Geophysicae*, *31*, 1–14.

Lund, T. S., & Fritts, D. C. (2012). Numerical simulation of gravity wave breaking in the lower thermosphere. *Journal of Geophysical Research*, *117*, 536. https://doi.org/10.1029/2012JD017

Marks, C. J., & Eckermann, S. D. (1995). A three-dimensional nonhydrostatic ray-tracing model for gravity waves: Formulation and preliminary results for the middle atmosphere. *Journal of the Atmospheric Sciences*, *52*, 1,952–1,984.

Oliver, W., Otsuka, Y., Sato, M., Takami, T., & Fukao, S. (1997). A climatology of F region gravity wave propagation over the middle and upper atmosphere radar. *Journal of Geophysical Research*, *102*, 14,499–14,512.

Pitteway, M. L. V., & Hines, C. O. (1963). The viscous damping of atmospheric gravity waves. *Canadian Journal of Physics*, *41*, 1,935–1,948.

Snively, J. B., & Pasko, V. P. (2008). Excitation of ducted gravity waves in the lower thermosphere by tropospheric sources. *Journal of Geophysical Research*, *113*, A06303. https://doi.org/10.1029/2007JA012693

Torrence, C., & Compo, G. P. (1998). A practical guide to wavelet analysis. *Bulletin of the American Meteorological Society*, *79*(1), 61–78.

Vadas, S. L. (2007). Horizontal and vertical propagation and dissipation of gravity waves in the thermosphere from lower atmospheric and thermospheric sources. *Journal of Geophysical Research*, *112*, A06305. https://doi.org/10.1029/2006JA011845

Vadas, S. L. (2013). Compressible F-plane solutions to body forces, heatings, and coolings, and application to the primary and secondary gravity waves generated by a deep convective plume. *Journal of Geophysical Research: Space Physics*, *118*, 2,377–2,397. https://doi.org/10.1002/jgra.50163

Vadas, S. L., & Fritts, D. C. (2002). The importance of spatial variability in the generation of secondary gravity waves from local body forces. *Geophysical Research Letters*, *29*(20), 1984. https://doi.org/10.1029/2002GL015574

Vadas, S. L., & Fritts, D. C. (2005). Thermospheric responses to gravity waves: Influences of increasing viscosity and thermal diffusivity. *Journal of Geophysical Research*, *110*, D15103. https://doi.org/10.1029/2004JD005574

Vadas, S. L., & Fritts, D. C. (2006). Influence of solar variability on gravity wave structure and dissipation in the thermosphere from tropospheric convection. *Journal of Geophysical Research*, *111*, A10S12. https://doi.org/10.1029/2005JA011510

Vadas, S. L., & Fritts, D. C. (2009). Reconstruction of the gravity wave field from convective plumes via ray tracing. *Annales Geophysicae*, *27*, 147–177.

Vadas, S. L., Fritts, D. C., & Alexander, M. J. (2003). Mechanism for the generation of secondary waves in wave breaking regions. *Journal of the Atmospheric Sciences*, *60*, 194–214. https://doi.org/10.1175/1520-0469(2003)060)

Vadas, S. L., & Liu, H. L. (2009). Generation of large scale gravity waves and neutral winds in the thermosphere from the dissipation of convectively generated gravity waves. *Journal of Geophysical Research*, *114*, A10310. https://doi.org/10.1029/2009JA014108

Vadas, S. L., & Liu, H. L. (2013). Numerical modeling of the large-scale neutral and plasma responses to the body forces created by the dissipation of gravity waves from 6 h of deep convection in Brazil. *Journal of Geophysical Research: Space Physics*, *118*, 2,593–2,617. https://doi.org/10.1002/jgra.50249

Vadas, S. L., Liu, H.-L., & Lieberman, R. S. (2014). Numerical modeling of the global changes to the thermosphere and ionosphere from the dissipation of gravity waves from deep convection. *Journal of Geophysical Research: Space Physics*, *119*, 7,762–7,793. https://doi.org/10.1002/2014JA020280

Vadas, S. L., Makela, J. J., Nicolls, M. J., & Milliff, R. F. (2015). Excitation of gravity waves by ocean surface wave packets: Upward propagation and reconstruction of the thermospheric gravity wave field. *Journal of Geophysical Research: Space Physics*, *120*, 9,748–9,780. https://doi.org/10.1002/2015JA021430

Vadas, S. L., & Nicolls, M. J. (2012). The phases and amplitudes of gravity waves propagating and dissipating in the thermosphere: Theory. *Journal of Geophysical Research*, *117*, A05322. https://doi.org/10.1029/2011JA017426

Vincent, R. A., Alexander, M. J., Dolman, B. K., MacKinnon, A. D., May, P. T., Kovalam, S., & Reid, I. M. (2013). Gravity wave generation by convection and momentum deposition in the mesosphere-lower thermosphere. *Journal of Geophysical Research: Atmospheres*, *118*, 6,233–6,245. https://doi.org/10.1002/jgrd.50372

Vincent, R. A., & Reid, I. M. (1983). HF DOppler measurements of mesospheric momentum fluxes. *Journal of the Atmospheric Sciences*, *40*, 1,321–1,333.

Walterscheid, R. L. (1981). Dynamical cooling induced by dissipating internal gravity waves. *Geophysical Research Letters*, *8*(12), 1235–1238. https://doi.org/10.1029/GL008i012p01235

Walterscheid, R (2013). The propagation of transient wave packets in highly dissipative media. *Journal of Geophysical Research: Space Physics*, *118*, 878–884. https://doi.org/10.1002/jgra.50097

Walterscheid, R. L., & Hecht, J. H. (2003). A reexamination of evanescent acoustic-gravity waves: Special properties and aeronomical significance. *Journal of Geophysical Research*, *108*(D11), 4340. https://doi.org/10.1029/2002JD002421

Waterscheid, R. L., & Hickey, M. P. (2011). Group velocity and energy flux in the thermosphere: Limits on the validity of group velocity in a viscous atmosphere. *Journal of Geophysical Research*, *116*, D12101. https://doi.org/10.1029/2010JD014987

Yiğit, E., Aylward, A. D., & Medvedev, A. S. (2008). Parameterization of the effects of vertically propagating gravity waves for thermosphere general circulation models: Sensitivity study. *Journal of Geophysical Research*, *113*, D19106. https://doi.org/10.1029/2008JD010135

Yiğit, E., & Medvedev, A. S. (2010). Internal gravity waves in the thermosphere during low and high solar activity: Simulation study. *Journal of Geophysical Research*, *115*, A00G02. https://doi.org/10.1029/2009JA015106

Yiğit, E., & Medvedev, A. S. (2015). Internal wave coupling processes in Earth's atmosphere. *Advances in Space Research*, *55*, 983–1,003. https://doi.org/10.1016/j.asr.2014.11.020

Yiğit, E., Medvedev, A. S., Aylward, H. P., Hartogh, P., & Harris, M. J. (2009). Modeling the effects of gravity wave momentum deposition on the general circulation above the turbopause. *Journal of Geophysical Research*, *114*, D07101. https://doi.org/10.1029/2008JD011132

Zhang, S. D., & Yi, F. (2002). A numerical study of propagation characteristics of gravity wave packets propagating in a dissipative atmosphere. *Journal of Geophysical Research*, *107*, 4,222. https://doi.org/10.1029/2001JD000864